

**URTeC: 2697500**

## **Quantification of Recovery Factors in Downspaced Shale Wells: Application of a Fully Coupled Geomechanical EOS compositional Simulator**

Saurabh Sinha and Deepak Devegowda\*, University of Oklahoma; Bhabesh Deka

Copyright 2017, Unconventional Resources Technology Conference (URTeC) DOI 10.15530/urtec-2017-2697500

This paper was prepared for presentation at the Unconventional Resources Technology Conference held in Austin, Texas, USA, 24-26 July 2017.

The URTeC Technical Program Committee accepted this presentation on the basis of information contained in an abstract submitted by the author(s). The contents of this paper have not been reviewed by URTeC and URTeC does not warrant the accuracy, reliability, or timeliness of any information herein. All information is the responsibility of, and, is subject to corrections by the author(s). Any person or entity that relies on any information obtained from this paper does so at their own risk. The information herein does not necessarily reflect any position of URTeC. Any reproduction, distribution, or storage of any part of this paper without the written consent of URTeC is prohibited.

### **Abstract**

The contribution from outside the Stimulated Rock Volume (SRV) to well performance is generally limited in shale wells (Ambrose et al. 2011) necessitating optimal well and fracture spacing. The well spacing is often also governed by the recovery factors per well or recovery factors per lease in the case of PAD wells. In this work, we quantify recovery factors for downspaced shale wells using a reservoir simulation approach supported by rate transient analysis (RTA) and geomechanical and petrophysical studies.

Our analyses is based on data from a PAD well in the Eagle Ford shale. First we identify different petrofacies in the area of study from well logs. These are then populated in a 3D reservoir simulation model with the corresponding rock type (RC) constrained porosity and water saturation. Permeability estimates are derived from an RTA-based workflow. The well is completed in the rich gas condensate window of the Eagle Ford and an equation of state (EOS) model is calibrated to available laboratory data.

To mimic the fracturing process we have implemented the modified Barton-Bandis model in flow simulation suggested by Tran et al. (2009) to model the opening and closing of fractures and the corresponding effective stress changes during injection/production. We couple the geomechanical model iteratively into the flow model to solve for both stresses and fluid flow in the reservoir and history match gas rates, condensate rates, water rates and flowing bottomhole pressure (FBHP) simultaneously.

We use the history matched model to run sensitivities for both upspacing and downspacing scenarios with respect to conventional 500 ft. spacing. In all sensitivity scenarios, we monitor the growth of fractures with the actual pumping schedule to investigate fracture growth and possible completion strategies. Finally, we summarize our results for downspacing and upspacing of wells. Our results show that the optimal well spacing in the area of study in the Eagle Ford is 420 Ft.

### **Methodology**

#### **Static Model**

Our model consists of a PAD well in the Eagle Ford shale. The model contains three other wells on a PAD and offset pilot well logs in the area. Figure 1 shows the location of the PAD wells and the offset wells that were used to build the rock type model. For defining our rock types, we combined density porosity, neutron porosity, resistivity and gamma ray logs. These rock types are distributed through the reservoir model using sequential indicator simulation (SIS). We map the thickness of each rock type and create a rock type-specific thickness map. We then define the variograms for each rock type for the porosity variations.

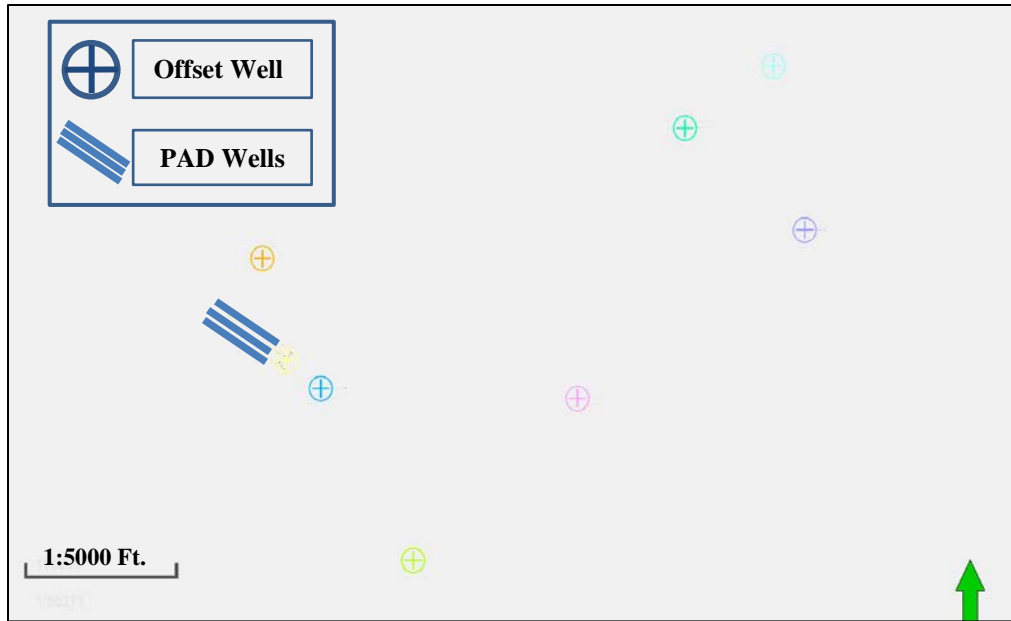


**Figure 1. Location of PAD and offset wells. The wells on the PAD are shown by solid blue lines and the offset wells are shown in circle with a cross. The PAD wells are horizontal multi fractured wells and the offset well logs are vertical pilot wells.**

Next, we used facies constrained Sequential Gaussian Simulation (SGS) to populate petrophysical properties calculated from well logs into the SIS rock type model. Figures 2 and 3 show the final rock type-constrained porosity and water saturation. We use the iterative formulation of the Simandoux equation suggested by Doveton (2001) to calculate the water saturations.

Matrix permeability is initialized using RTA with median permeability of 116 nD and a standard deviation of 35 nD. The upper, middle and lower Eagle Ford were then identified using trends from bulk density and resistivity following the methodology described by Workman (2013). In our area, the lower Eagle Ford is characterized by a higher porosity and lower water saturation indicating higher reservoir quality.

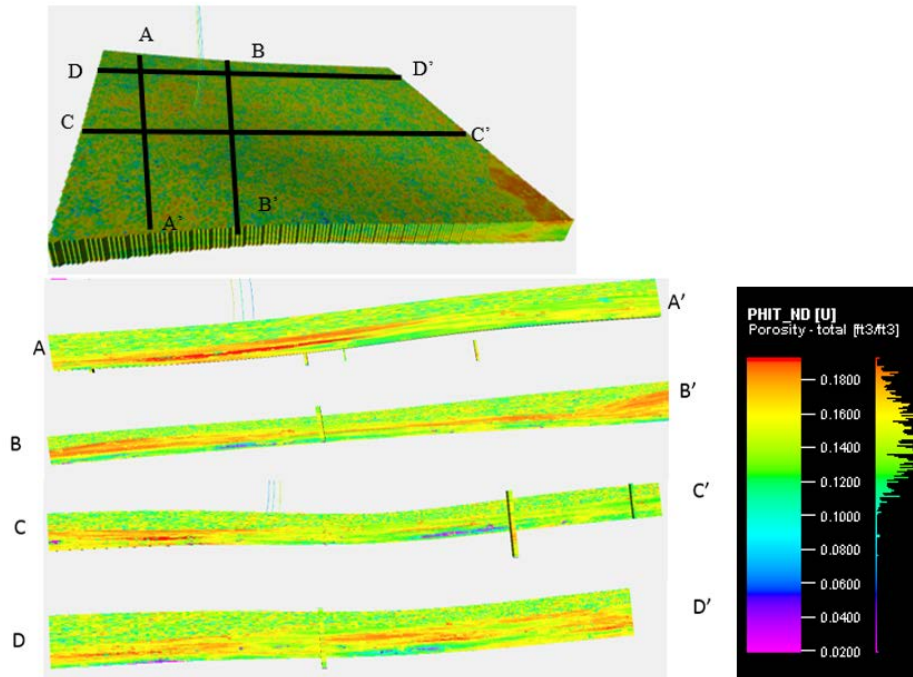


**Figure 2. Lithology constraint porosity model from 4 rock types. Separate cross sections show the porosity distribution around the wells in upper, middle and lower Eagle Ford zones. Porosity lies between 9% -18% with lower Eagle Ford showing higher porosity around the PAD wells. (Sinha et al. 2017)**

### Fluid Model

A fully compositional model is incorporated in the model and the EOS was calibrated to the constant composition experiment (CCE), depletion experiment and separator tests. The reservoir fluid is a rich condensate fluid with a dew point of 4284 psig at reservoir temperature. The critical point for our fluid is 258.7 °F and 4296 psig.

### Geomechanical Modeling

To model the stresses, a full geomechanical model coupled to our flow grid is used. The geomechanical simulator computes pressure and stresses and provides input to the flow grid that then solves the flow equations with a methodology suggested by Islam and Settari (2013) and Ji et al. (2009). We use a modified Barton-Bandis semi-logarithmic closure model (Bandis et al. 1983) previously used by Tran et al. (2009) to model the fracture opening and closing with injection and production respectively. To model the injection during the fracturing, post fracturing reports are used for rates and pressure at every stage.

To model stagewise injection, perforations corresponding to a stage are opened while the rest are closed, and the process is repeated from the toe to the heel of the well in 12 different stages. The average fluid rate in our case is 70 BPM per perforation cluster. The vertical stress is initialized by the following equation:

$$\sigma = \sigma' + \alpha p \quad (1)$$

This is the 1 D stress equation, where:  $\sigma$  is the total stress,  $\sigma'$  is the effective stress,  $\alpha$  is the Biot's coefficient and  $p$  is the pore pressure.

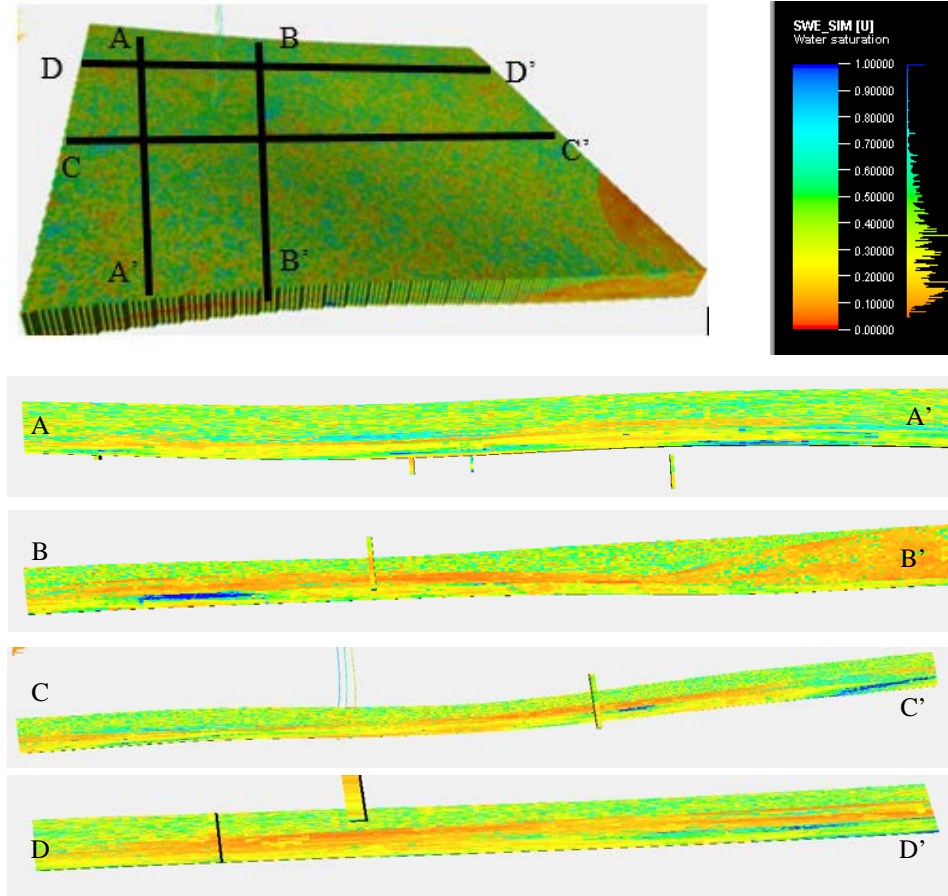


**Figure 3. Lithology constraint water saturation model. Separate cross sections show the saturation distribution around the PAD wells in upper, middle and lower Eagle Ford. It can be observed that the lower Eagle Ford shows lower water saturation around the PAD wells modeled in the study (after Sinha et al. (2017)).**

We calculated the density by integrating the bulk density log and used it to calculate the overburden stress. Then using Equation 1 we calculate the initial effective stress for undrained condition. The Biot number of 0.86 was chosen from a static test reported by Mokhtari et al. (2014) in La Salle county, TX. We assumed a constant water column of 0.45 psi/ft. for our calculations. To initialize the horizontal stresses, the maximum and minimum horizontal stresses are calculated from well logs and poro-elastic strain equations with the methodology suggested by Herwanger et al. (2015). We iterate over equations (2) and (3) with a goal seek criterion until the stresses match the pump pressures reported.

$$\sigma_{hmin} = \frac{\vartheta}{1-\vartheta}(\sigma_v - \alpha P_p) + \frac{E}{1-\vartheta^2} \epsilon_{hmin} + \frac{E\vartheta}{1-\vartheta^2} \epsilon_{Hmax} + \alpha P_p \quad (2)$$

$$\sigma_{hmax} = \frac{\vartheta}{1-\vartheta}(\sigma_v - \alpha P_p) + \frac{E}{1-\vartheta^2} \epsilon_{hmax} + \frac{E\vartheta}{1-\vartheta^2} \epsilon_{Hmin} + \alpha P_p \quad (3)$$

Where  $\sigma_{hmin}$  and  $\sigma_{hmax}$  are the minimum and maximum horizontal stresses,  $\epsilon_{hmax}$  and  $\epsilon_{hmin}$  are the maximum and minimum strain,  $E$  is Young's modulus,  $\alpha$  is Biot's constant,  $P_p$  is pore pressure, and  $\sigma_v$  is the vertical overburden stress. The modified Branton-Bandis model described by Tran et al. (2009) with fracture permeability plotted against the effective stress is shown in Figure 4 and the model parameters are listed in Table 1. With injection during the fracturing process, the actual effective stress decreases from point A towards point B. Tensile failure occurs at point B and permeability increases dramatically to point C. Once injection stops, and wells are brought on production the effective stress increases again (Equations 1 through 3); however the fracture retains a

permeability  $K_{\min}$  as the propped fracture conductivity. We used  $K_{\min}$  as a history matching parameter later in the study to match the well flowing bottomhole pressure (WFBHP).

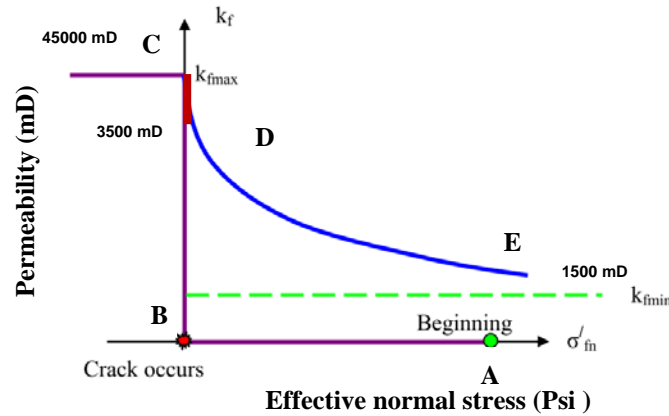


**Figure 4. Modified Barton-Bandis model used in the simulation study (modified after Tran et al., 2009). Rock failure occurs at point B and hydraulic fracture is created to an increased permeability to point C. As the pumps at the surface stop at point C, the stress increases and the permeability starts to decrease to point D (during shut-in before flow back). During production, the permeability further decreases to finally permeability of propped open fracture. The curve from D to E explains the initial flash production.**

### History Matching

Results from the base case model with 500 ft. well spacing for simultaneous matching of gas rate, oil rate, flowing bottomhole pressure and water rate are shown in Figure 5. An excellent match is obtained on all parameters except WFBHP. Hence, to match WFBHP an unconventional history matching methodology is followed.

The parameters which are uncertain are: relative permeability curves, initial reservoir pressure, fracture stiffness and residual fracture permeability. These were selected by conducting a sensitivity analyses on several variables and selecting the ones with the highest impact on WFBHP pressure for history matching. We create a global objective function containing rates and well FBHP's to minimize the error in the actual field history vs. simulated production. For optimization, we use particle swarm optimization (Kennedy and Eberhart, 1995) to minimize the global error function. Different weights were assigned to different data types to reflect the uncertainty in the measurements. This is a subjective choice and requires user judgement.

**Table 1. Values used to initialize the geomechanical model.**

Parameter	Value
Initial fracture aperture	0.0001 Ft.
Initial fracture stiffness	2.52 E06
Initial fracture opening stress (limiting case)	5800 psi
Initial hydraulic fracture permeability	45000 mD
Fracture closure permeability	3500 mD
Initial increased residual permeability	1500 mD

We finally construct a proxy model from history matched (HM) global optimization results to minimize the error in WFBHP keeping the match on oil rates intact. Our model is running on gas rate control for history matching and constant flowing pressures afterwards. The final history match is shown in Figure 6.

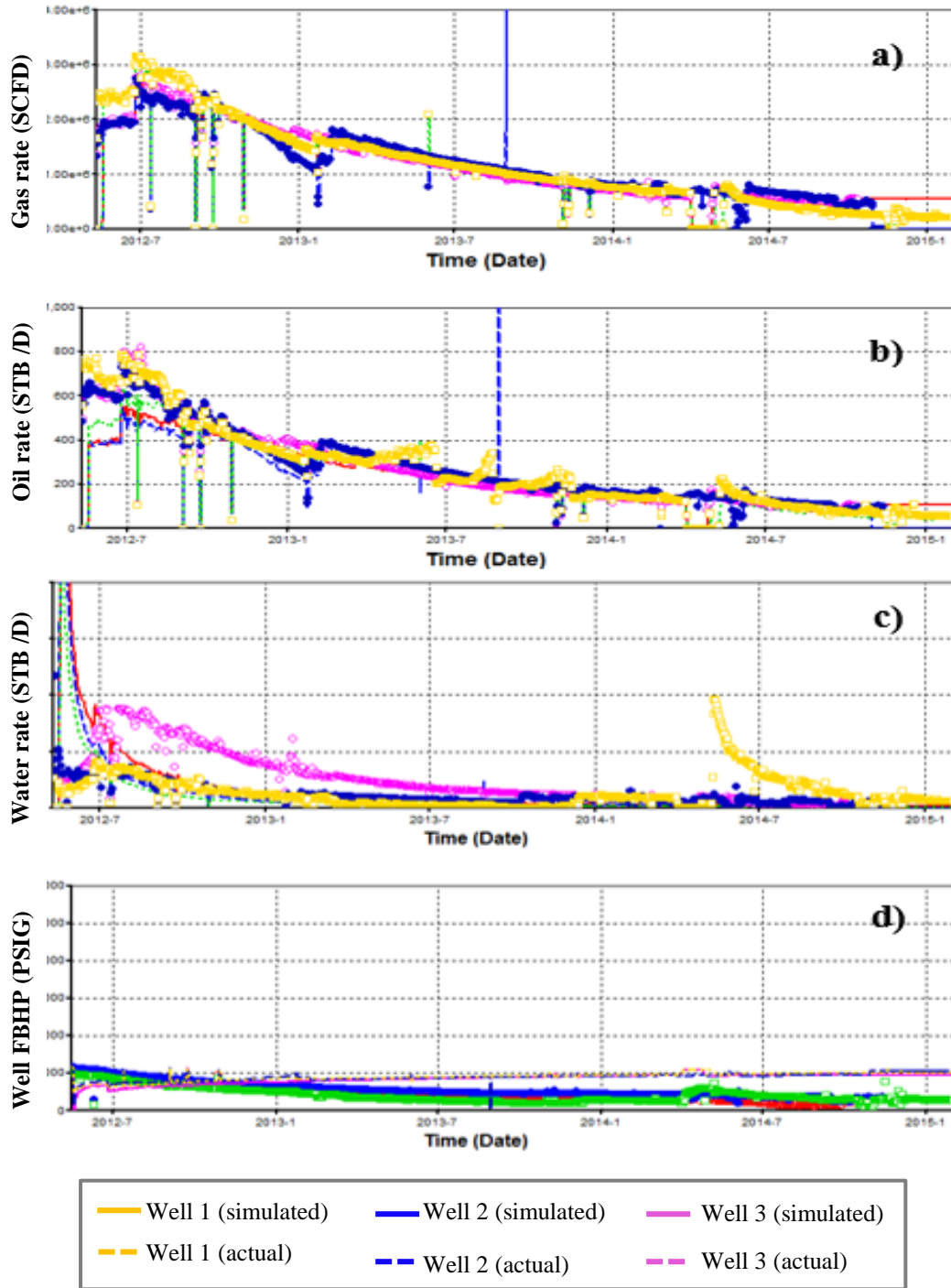
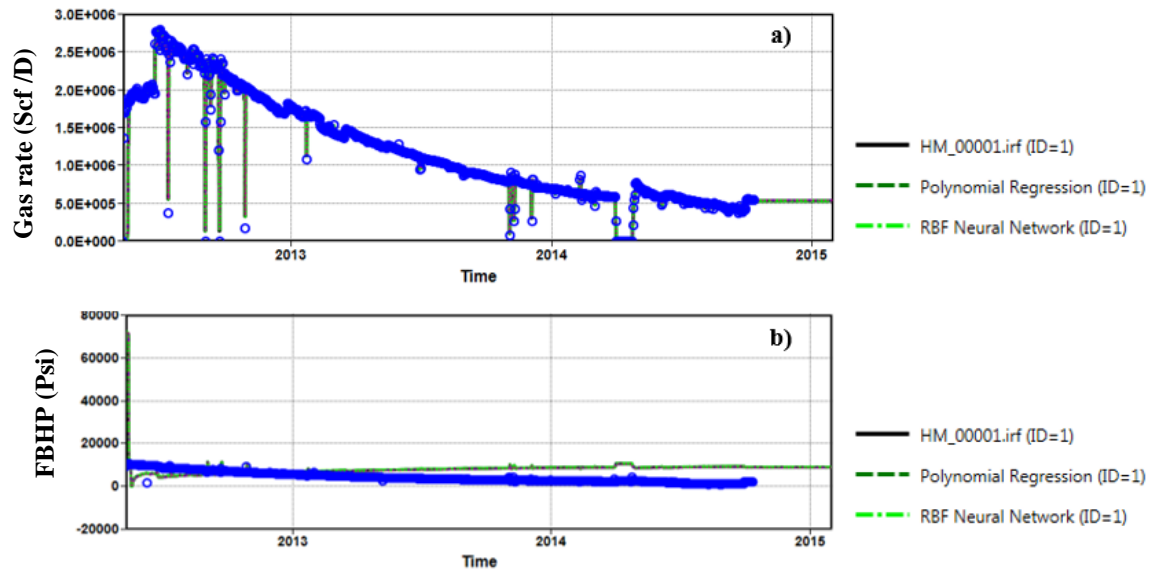


Figure 5. Initial simulation history match. From top to bottom a) gas rate b) oil rate c) water rate d) well flowing bottomhole pressure. Well is running on gas rate control for history matching period and constant drawdown of 3500 psi afterwards (dew point of the fluid is 4284 psi). The increased water rate in well 1 after 2 years is due to a refracturing job.



**Figure 6. Example gas rate for well 1, out of three wells on the PAD. Figure a) shows the gas rate and Figure B shows the WFBHP. Blue curve is field history, and the black curve is initial history match from minimization of global error using particle swarm optimization. The dark green dashed line is the polynomial proxy model prediction and the light green is the neural net proxy model. It can be observed that the match improved on WFBHP while keeping the match on gas rate intact. The matched values of fracture conductivity and relative permeability is then used for prediction.**

#### Sensitivity Cases and associated assumptions

After a satisfactory history match is obtained, sensitivity studies around the history matched model (henceforth called the base case scenario) is conducted. We assume that the completion design (such as injection volumes, rates, proppant volume and fluid volumes) remain the same for upspacing and downspacing scenarios.

Results from upspacing and downspacing with respect to the base case scenario are summarized in Table 2. Volumetric considerations provide the original gas in place (OGIP) assuming a square lease (Sinha et al., 2017). Recovery factors are reported for the major phase which is gas. For the upspacing scenarios, assuming the same SRV, the OGIP is fixed at 39 BSCF. Under these assumptions, the optimal well spacing is 420' in the area of study. All expected ultimate recoveries (EUR's) reported in Table 2 are for a well life of 30 years. For the base case study, the EUR's reported are averaged for three wells on the PAD. The middle well from the three well PAD showed a higher EUR in comparison to the other two adjacent wells.

Because we have reported the recovery factors per lease for the major phase, the maximum recovery factor at 420' suggests that an operator with an initial well spacing of 500' with 5 wells in a 2500' X 2500' lease will now be able to place an additional well per lease without compromising recovery factors. Going below the 420' spacing may require extra reserves deduction on account of well interference.

**Table 2. Recovery factor versus well spacing. Recovery factor is a maximum at 420 ft. well spacing.**

Well Spacing (Ft.)	Oil EUR (MSTB)	Gas EUR(BSCF)	OGIP(BSCF)	Gas Recovery Factor	
280	185	3.4	22	15.45%	
<b>420(optimal)</b>	<b>320</b>	<b>5.57</b>	<b>33</b>	<b>16.8%</b>	
<b>500 (base case)</b>	<b>335</b>	<b>5.35</b>	<b>39</b>	<b>14.49%</b>	
700	375	6.21	39	15.9%	
840	365	6.32	39	16.20%	
980	386	6.29	39	16.12%	

## Results and Conclusions

Our results show that the optimal spacing in case of downspaced wells in the rich condensate area of the Eagle Ford shale is 420 ft. We observed an uneven fracture growth across the different sections of the lateral. Figure 7 shows the effective normal stress and the pressure depletion. Figure 8 shows the associated volumetric strain. The stress regimes of the wells are dynamic and change with injection. Hence, different stages show different effective normal stresses as seen in Figure 9.

The fracture grows up to the top of Eagle Ford initially and matches more or less with the microseismic volume. Figure 10 shows this in 3D. Figure 10 (a) shows the 3D view of the fracture growth with flow model coupled with Barton-Bandis model. Figure 10 (b) shows the SRV generated using microseismic events after applying amplitude filters to extract microseismic related events only with the methodology suggested by Suliman et al. (2013).

The model shows uneven drainage areas with some stages interfering with each other while leaving some area undrained between the other stages. This is illustrated in Figure 11 with different cross sections (A-A' and B-B' as seen in Figure 11a) of the model showing undrained areas thereby suggesting the 500' well spacing is not optimal.

We also suspect that there might be secondary and tertiary stems to the Barton-Bandis model which can further lower the fracture conductivity below  $K_{min}$  thereby necessitating re-fracturing. These effects are indicated in the latter portion of the bottomhole pressure trends. We are able to match the initial and the middle portion of the FBHP accurately, but later trends in bottomhole pressure show a sharp declining trend. One possible explanation is gradual fracture closure beyond the residual permeability in Barton-Bandis model. Due to insufficient well history we are unable to model this effect and will focus on this effect in future work.

One of the advantages of our workflow is that we are able to assess changing completion parameters coupled with a geomechanical model to decide between staggered and same layer completions. It is also useful to determine well placement at a later stage in field development to target undrained regions. We have observed that the Barton-Bandis model is sufficient to model the initial flash production and a large proportion of subsequent well life except for the tail end of the production. For a majority of operators, this period of production can be decisive to opt for one completion scheme or the other due to economics.

Our model simulates the Barton-Bandis effect, by a forward modeling approach which includes generating a dynamic SRV from the geomechanical model and then use it for history matching instead of the methodology suggested by Suliman et al. (2013). The latter, generates fracture networks from microseismic data or other acoustic events suggested by Patel et al. (2017), and hence does not capture the fracturing phenomenon as a function of injection volumes and hence cannot be used as a forecasting and decision making tool.

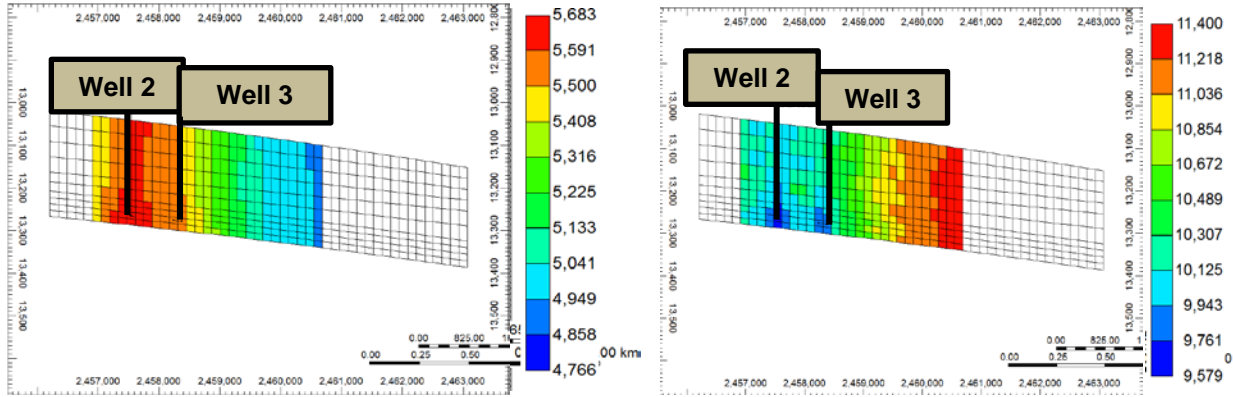


**Figure 7.** Two wells (well 1 and Well 3 in IK view) which are 500 Ft. apart from each other. On the left is the effective normal stress(psi) and on the right is the reservoir pressure (psi) two months into production. Notice that for well 1 the fractures are closing rapidly due to increased effective stress and hence a short-lived flash production. Same is observed for second image although the primary depletion is mainly restricted to lower Eagle Ford. Top five layers in z direction are upper + middle EFS and bottom 5 layers are lower Eagle Ford. All wells are choke managed.

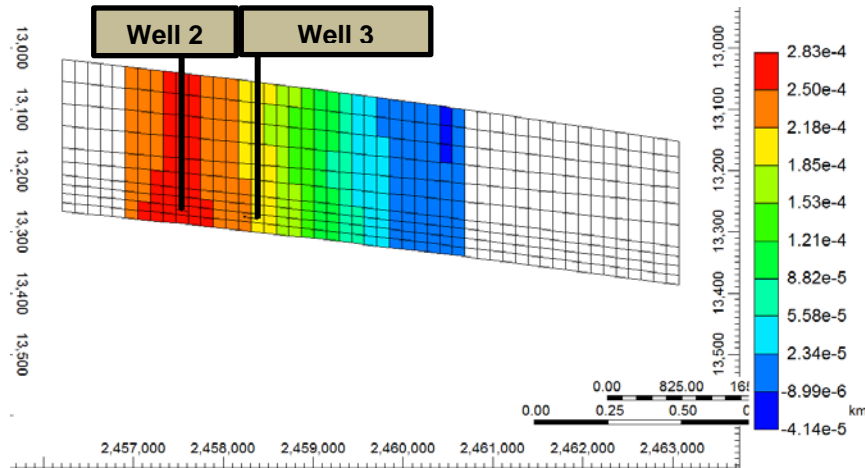


**Figure 8.** Volumetric strain in the reservoir. Uneven volumetric strain across the reservoir show uneven fracture growth and hence uneven depletion in the reservoir.

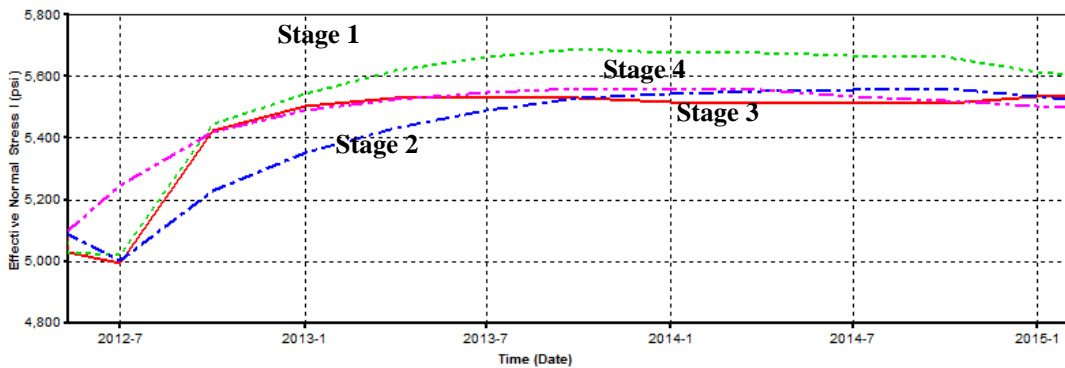


**Figure 9.** Effective normal stress from 4 different stages out of 12 stages of well 1. Barton-Bandis effect can be observed in stress trends. All stages show different stress regimes suggesting different fracture growth with dynamic stress profiles. This can have a significant effect and explains the zipper fracturing effect i.e. middle well usually show higher SRV than edge wells on a PAD due to stress redistribution.

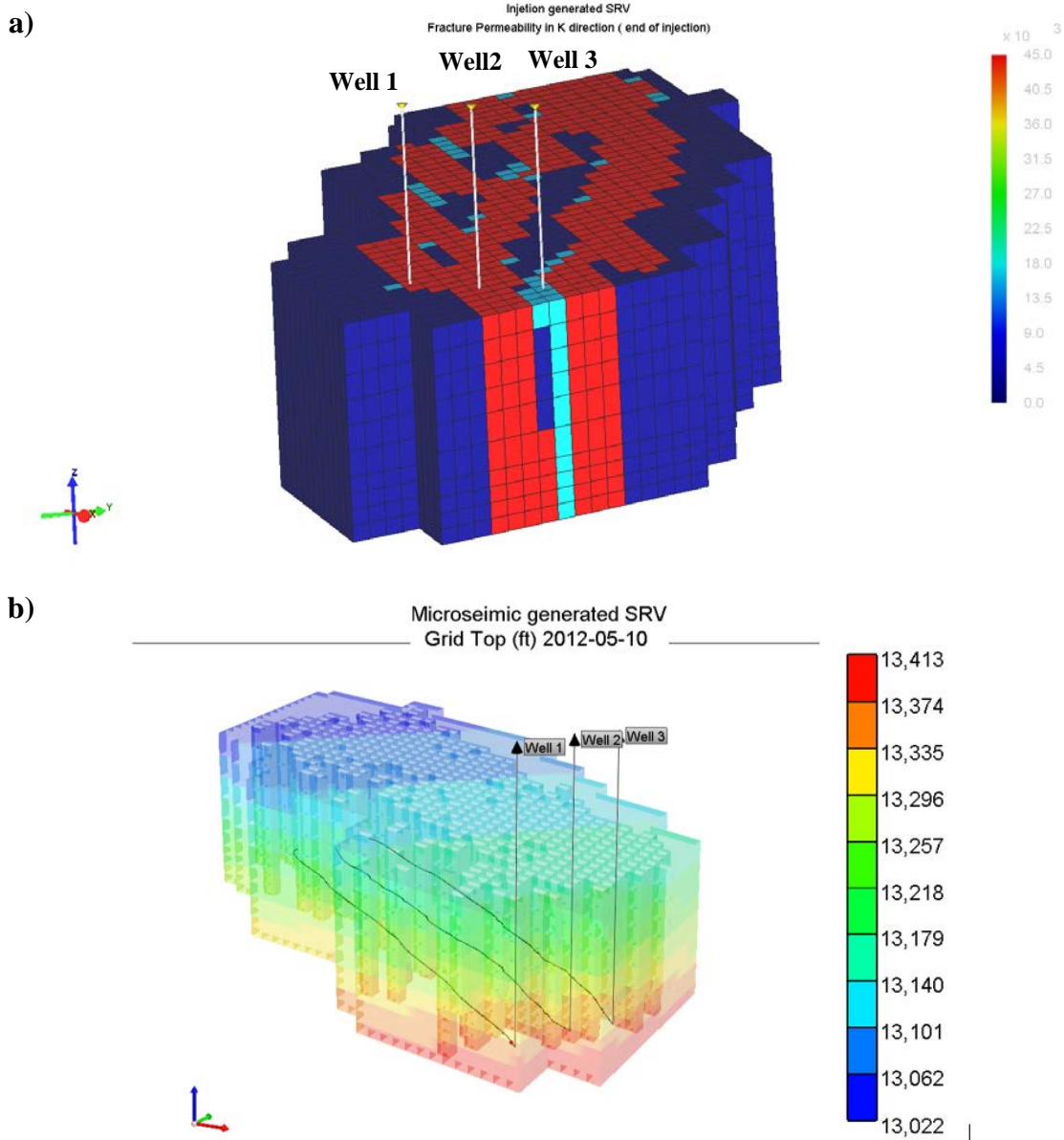


**Figure 10. a) SRV generated using coupled model with the actual injection schedule b) SRV generated using grid refinement using microseismic data. Both SRV look similar in the beginning. However, the latter is fixed and overestimates the SRV. The former has initial SRV which is dynamic and changes with stress alteration with production.**

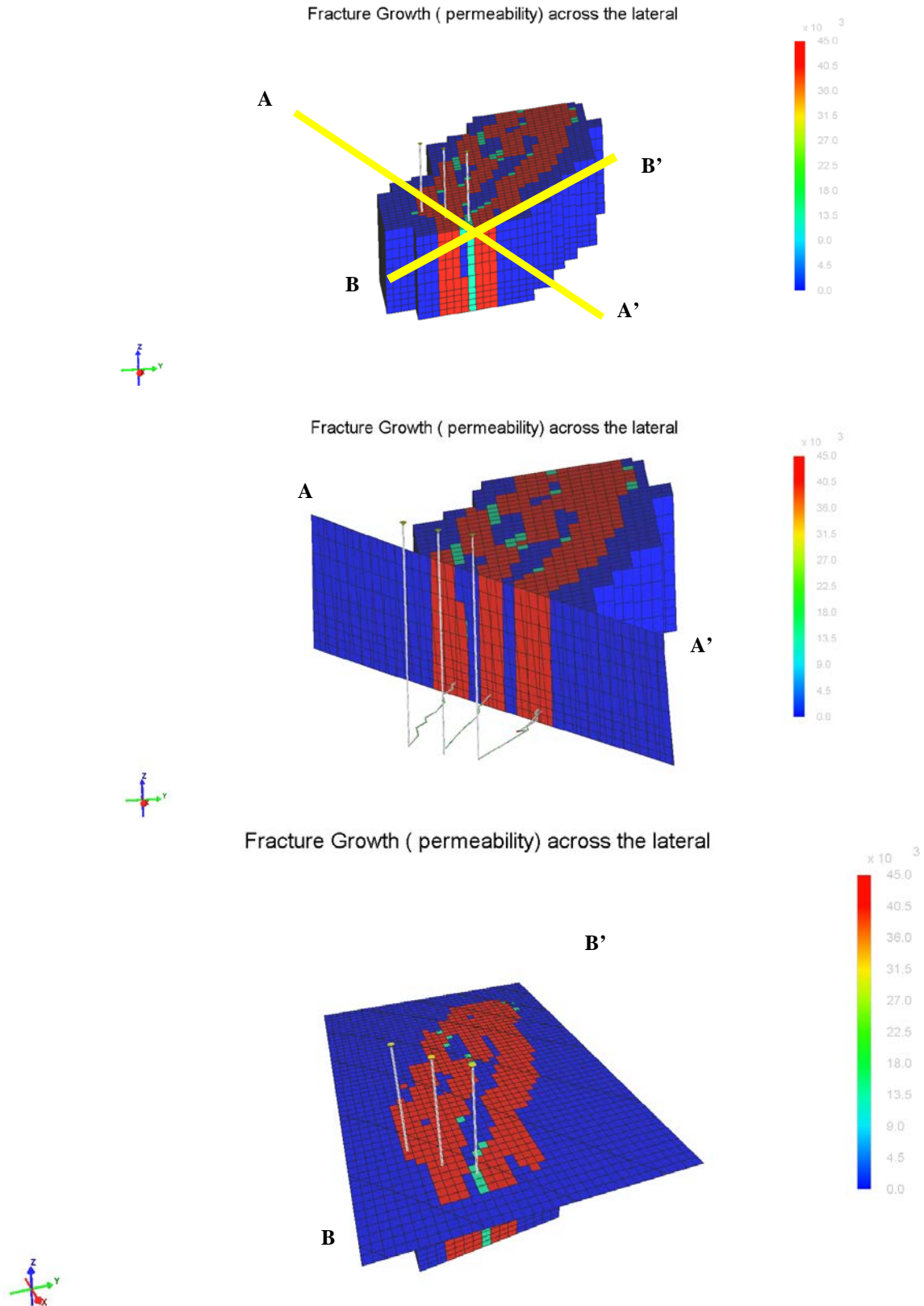


**Figure 11. Final SRV after injection and different cross sections along the lateral. A-A' is a vertical cross-section while B-B' is a horizontal cross-section. It can be observed that the SRV is uneven across the lateral as well as across the EFS section. (Upper versus lower EFS)**

We have observed uneven drainage areas which is shown in Figure 11. Hence, a recovery factor approach based on a bi-wing fracture geometry is insufficient to quantify the recovery factors. In a conventional RTA based approach these uneven drainage areas will collapse into a square boxlike SRV with fracture half lengths. This obviously will lead to an incorrect interpretation of well spacing. Hence, although a good starting point to initialize the matrix permeability, we strongly suggest using the coupled simulation-based approach instead of a boxlike SRV.

One limitation of our model is the initial stress anisotropy across the lateral length that we are unable to model. We instead relied on the use of a constant principal stress across the area.

### Acknowledgements

We would like to thank Tanh Nguyen and K Patel from Computer Modelling Group (CMG®) for their technical support and generous contribution of their software licenses to University of Oklahoma(OU).

### Nomenclature

$\sigma$	Total stress
$\sigma'$	Effective stress
$\alpha$	Biot's coefficient
$P_p$	Pore pressure
$\sigma_{hmin}$	Minimum horizontal effective stress
$\sigma_{Hmax}$	Maximum horizontal effective stress
$\epsilon_{Hmax}$	Maximum strain
$\epsilon_{hmin}$	Minimum strain
$E$	Young's modulus
$\sigma_v$	Vertical overburden stress

### References

- Ambrose, Ray J, Devon Energy, C R Clarkson, Jerry Youngblood, Rod Adams, Phuong Nguyen, M Nobakht, and Brent Biseda. 2011. "Life-Cycle Decline Curve Estimation for Tight / Shale Gas Reservoirs." *Society*, no. 2008: 607–621, SPE 140519. doi:10.2118/140519-MS.
- Bandis, S. C., A. C. Lumsden, and N. R. Barton. 1983. "Fundamentals of Rock Joint Deformation." *International Journal of Rock Mechanics and Mining Sciences and* 20 (6): 249–68. doi:10.1016/0148-9062(83)90595-8.
- Devegowda D., Deka B. Sinha S. 2017. "SPE-185748\_Saurabh\_sinha." In *Quantification of Recovery Factors in Downspaced Wells: Application to the Eagle Ford Shale*. SPE-185748.
- Doveton, John H. 2001. "All Models Are Wrong , but Some Models Are Useful : ‘ Solving ’ the Simandoux Equation Prolog : The Archie Equation."
- Hamada, G M, The British, A A Almajed, and King Fahd. 2010. "Uncertainly Analysis of Archie  $\hat{\epsilon}^{\text{TM}}$  S Parameters Determination Techniques in Carbonate Reservoirs Calculation of Archie  $\hat{\epsilon}^{\text{TM}}$  S Parameters," 1–10.
- Herwanger, Jorg V, Andrew D Bottrill, and Scott D Mildren. 2015. "Uses and Abuses of the Brittleness Index With Applications to Hydraulic Stimulation." *Unconventional Resources Technology Conference (URTeC)* 2172545 (2008): 1–9. doi:10.15530/urtec-2015-2172545.
- Islam, Arshad, and Antonin Settari. 2013. "Injection Modeling and Shear Failure Predictions in Tight Gas Sands — A Coupled Geomechanical Simulation Approach." *Effective and Sustainable Hydraulic Fracturing*. doi:10.5772/56312.
- Ji, Lujun, Antonin Settari, and Richard B Sullivan. 2009. "A Novel Hydraulic Fracturing Model Fully Coupled With Geomechanics and Reservoir Simulation." *SPE Journal* 14 (3): 423–30. doi:10.2118/110845-PA.
- Kennedy, J, and R Eberhart. 1995. "Particle Swarm Optimization." *Neural Networks, 1995. Proceedings., IEEE International Conference on* 4: 1942–48 vol.4. doi:10.1109/ICNN.1995.488968.
- Mokhtari, Mehdi, Mehdi Matt Matt Honarpour, Azra Nur Tutuncu, and Gregory N. Boitnott. 2014. "Acoustical and Geomechanical Characterization of Eagle Ford Shale -Anisotropy, Heterogeneity and Measurement Scale." *SPE Annual Technical Conference and Exhibition*. doi:10.2118/170707-MS.
- Patel, S.M., C.H. Sondergeld, and C.S. Rai. 2017. "Laboratory Studies of Hydraulic Fracturing by Cyclic Injection." *International Journal of Rock Mechanics and Mining Sciences* 95 (February). Elsevier Ltd: 8–15. doi:10.1016/j.ijrmms.2017.03.008.

- Sondhi, Namrita. 2013. "Petrophysical Characterization of Eagle Ford Shale." *Journal of Chemical Information and Modeling* 53 (9): 1689–99. doi:10.1017/CBO9781107415324.004.
- Suliman, B., R. Meek, R. Hull, H. Bello, D. Portis, and P. Richmond. 2013. "Variable Stimulated Reservoir Volume ( SRV ) Simulation: Eagle Ford Shale Case Study." *Spe 164546*, 13. doi:10.2118/164546-MS.
- Tran, David, Vijay Shrivastava, Long Nghiem, and Bruce Kohse. 2009. "Geomechanical Risk Mitigation for CO<sub>2</sub> Sequestration in Saline Aquifers." *Proceedings of SPE Annual Technical Conference and Exhibition*, 1–18. doi:10.2118/125167-MS.
- Workman, Seth J. 2013. "Integrating Depositional Facies and Sequence Stratigraphy in Characterizing Unconventional Reservoirs in the Cretaceous (Cenomanian-Turonian) Eagle Ford Shale, South Texas." *GCAGS Transactions*.